Magnetic Resonance and Ultrasound Image Fusion Using a PALM Algorithm

Oumaima El Mansouri[1], Adrian Basarab[1], Fabien Vidal[1,2], Denis Kouamé [1], Jean-Yves Tourneret[1],
[1] University of Toulouse, IRIT, CNRS, INP-ENSEEIHT, Universit Paul Sabatier Toulouse 3, France
[2] CHU Toulouse, Obstetrics Gynecology Department, Paule de viguier Hospital Toulouse F-31059, France

***Abstract*—This paper studies a new fusion algorithm for magnetic resonance (MR) and ultrasound (US) images combining two inverse problems for MR image super-resolution and US image despeckling. A polynomial function is used to link the gray levels of the two imaging modalities. Qualitative and quantitative evaluations on experimental phantom data show the interest of the proposed algorithm. The fused image is shown to take advantage of both the good contrast and high signal to noise ratio of the MR image and the good spatial resolution of the US image.**

I. Statistical model for MR/US image fusion

A. Observation models

In several clinical applications (e.g.,[1]), MRI has the advantage of acquiring images with a large field of view, at the expense of a relatively low spatial resolution depending on the duration of the acquisition, of the order of 1 mm. In contrast to MRI, depending on the choice of the probe central frequency, US imaging can offer well-resolved images but contaminated by a high level of speckle noise and with a reduced field of view. These observations motivate the need of MR/US image fusion and in particular the algorithm proposed hereafter. To account for the properties of each imaging modality, the following two observations models are used [2], [3]

$$\begin{aligned} \mathbf{y}_{\mathrm{m}} &= \mathbf{S}\mathbf{H}\mathbf{x}_{\mathrm{m}} + \mathbf{n}_{\mathrm{m}} \\ \mathbf{y}_{\mathrm{u}} &= \mathbf{x}_{\mathrm{u}} + \mathbf{n}_{\mathrm{u}} \end{aligned} \tag{1}$$

where $\mathbf{x}_{\mathrm{m}} \in \mathbb{R}^N$ is the non-observable high-resolution MR image, $\mathbf{y}_{\mathrm{m}} \in \mathbb{R}^M$ is the low-resolution observed MR image, $\mathbf{n}_{\mathrm{m}} \in \mathbb{R}^N$ is an independent identically distributed (i.i.d.) additive white Gaussian noise with variance σ_{m}^2, $\mathbf{H} \in \mathbb{R}^{N\times N}$ is a block circulant with circulant blocks matrix modelling the blurring effect of the MRI point spread function (PSF) with circulant boundary conditions, $\mathbf{S} \in \mathbb{R}^{M\times N}$ (with $N = d^2M$) is a decimation operator with a decimation factor d. On the other hand, $\mathbf{y}_{\mathrm{u}} \in \mathbb{R}^N$ is the observed B-mode US image, $\mathbf{x}_{\mathrm{u}} \in \mathbb{R}^N$ is the noise-free US image and $\mathbf{n}_{\mathrm{u}} \in \mathbb{R}^N$ is an i.i.d. additive log-Rayleigh noise sequence with localization parameter γ.

B. Relation between US and MR images

Because they exploit different physical phenomena within the acquisition process, MR and US images are not identical, even in the ideal case where they represent the same tissues without any distortion and without noise. The differences of gray levels between the two modalities are modelled in this study by a polynomial function, as suggested in [4] for MR/US image registration. This model originates from the observation that US images are formed due to the interfaces between anatomical structures having different acoustic impedances, which are related to the gradient of the MR image, *i.e.*,

$$\mathbf{x}_{\mathrm{u}} = f(\mathbf{x}_{\mathrm{m}}, \nabla\mathbf{x}_{\mathrm{m}}^{\mathbf{H}}\mathbf{u})$$

where $f : \mathbb{R}^{\mathbb{N}} \times \mathbb{R}^{\mathbb{N}} \to \mathbb{R}^{\mathbb{N}}$ is an unknown function, $\mathbf{u}$ is the scan direction and ∇ is the discrete gradient operator. Interesting registration results were obtained in [4] by choosing f as a polynomial function leading to

$$x_{u,i} = \sum_{p+q\leq 3} c_{pq} x_{m,i}^p (\nabla x_m^H u)_i^q \tag{2}$$

where c_{pq} are the unknown polynomial coefficients and $x_{u,i}$ and $x_{m,i}$ stand for the i^{th} sample of vectors $\mathbf{x}_{\mathrm{u}}$ and $\mathbf{x}_{\mathrm{m}}$. Note that according to Weierstrass theorem, any function can be approximated by a polynomial. Estimating $\mathbf{x}$ in the sense of the maximum *a posteriori* principle and assuming $\mathbf{x}$ is piecewise smooth leads to the following optimization problem

$$\begin{aligned} \hat{\mathbf{x}}_{\mathrm{m}} = \underset{\mathbf{x}}{\operatorname{argmin}} & \underbrace{\frac{1}{2}\|\mathbf{y}_{\mathrm{m}} - \mathbf{S}\mathbf{H}\mathbf{x}\|^2}_{\text{MRI data fidelity}} + \underbrace{\tau_1\|\nabla\mathbf{x}\|^2 + \tau_3\|\nabla f(\mathbf{x}, \nabla\mathbf{x}^{\mathbf{H}}\mathbf{u})\|^2}_{\text{regularization}} \\ & + \underbrace{\tau_2 \sum_{i=1}^{N} \Big[\exp(y_{\mathrm{u},i} - f_i(\boldsymbol{x}, \nabla x^H u)) - \gamma(y_{\mathrm{u},i} - f_i(\boldsymbol{x}, \nabla x^H u)) \Big]}_{\text{US data fidelity}} \end{aligned} \tag{3}$$

where τ_1, τ_2 and τ_3 are hyperparameters balancing the weight between the data fidelity term and the total variation (TV) regularization terms. The US data fidelity results from the log-Rayleigh distribution of the speckle [3].

II. MR/US image fusion

To solve (3), we propose to use the proximal alternating linearized minimization (PALM), adapted to nonconvex and nonsmooth functions [5]. In order to fit our image fusion to PALM framework, we introduce the auxiliary variable $\mathbf{v} = f(\mathbf{x}, \nabla\mathbf{x}^{\mathbf{H}}\mathbf{u})$, that transforms the fusion problem (3) in

$$\min_{(\mathbf{x},\mathbf{v})} \psi(\mathbf{x}, \mathbf{v}) := l(\mathbf{x}) + g(\mathbf{v}) + H(\mathbf{x}, \mathbf{v})$$

$$\begin{aligned} \text{where} \quad l(\mathbf{x}) &= \frac{1}{2}\|\mathbf{y}_{\mathrm{m}} - \mathbf{S}\mathbf{H}\mathbf{x}\|_2^2 + \tau_1\|\nabla\mathbf{x}\|^2 \\ g(\mathbf{v}) &= \tau_2 \sum_i [\exp(y_{\mathrm{u},i} - v_i) - \gamma(y_{\mathrm{u},i} - v_i)] + \tau_3\|\nabla\mathbf{v}\|^2 \\ H(\mathbf{x}, \mathbf{v}) &= \tau_4 \sum_{i=1}^{N} \left(v_i - \sum_{p+q\leq 3} c_{pq} x_i^p (\nabla x^H u)_i^q \right) \end{aligned}$$

The main steps of the fusion algorithm are given in Algo. 1, where k stands for the iteration number.

III. Results

The fusion algorithm was evaluated using an experimental dataset acquired from real images of a beef steak on top of which was glued a structure made by PolyVinyl Alcohol (PVA). The MR, US and fused images are shown in Fig. 1(a-c). The fused image highlight the ability of the proposed algorithm to provide an image having the good spatial resolution of US and the good contrast of MRI. This observation is confirmed by the contrast to noise ratios in Tab. 1, by the image profiles in Fig. 1(d) and by their slopes in Tab. 2. An interesting prospect is to study the robustness of the proposed algorithm to registration errors.

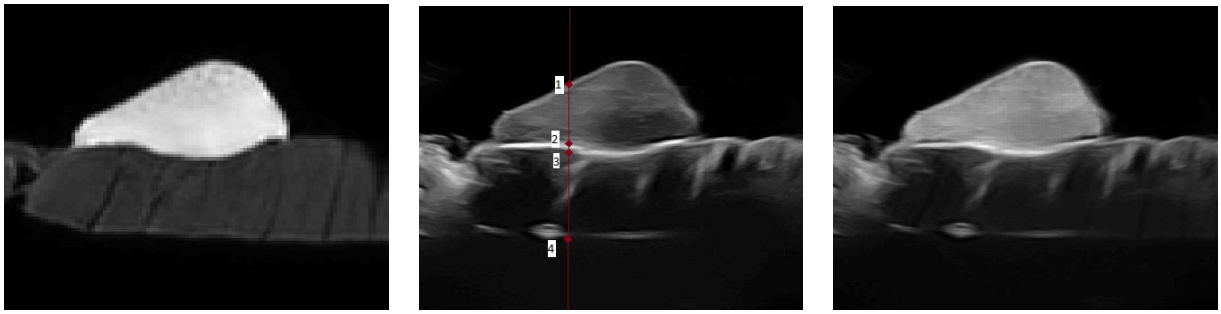

(a) MRI observation (b) US observation (c) Fused image

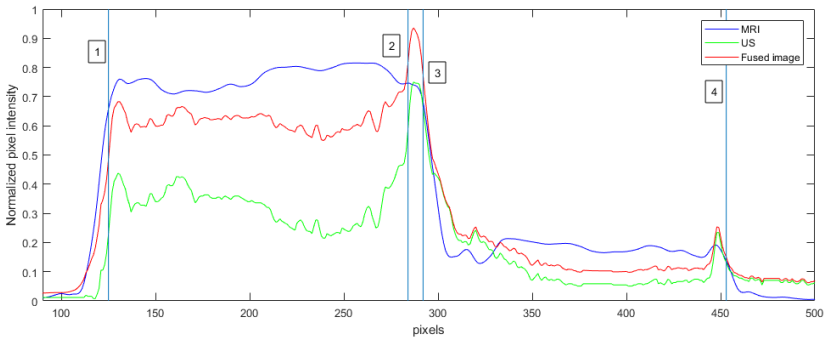

(d)

Fig. 1: (a) MR image, (b) US image, (c) fused MR and US image with the proposed algorithm, (d) normalized profiles corresponding to the vertical line in (b) extracted from the MR, US and fused images. Note that the three main visible structures, from top to bottom are, the PVA phantom, the glue and the beef steak. Because of the low resolution, the glue is not visible in the MR image. Because of the low contrast, the PVA and the beef steak have similar gray levels in the US image. The fused image achieves a good compromise between the observed MRI and US images.

Algorithm 1: Proposed MR/US image fusion algorithm.

Input $\mathbf{y_u}$, $\mathbf{y_m}$, $\mathbf{S}$, $\mathbf{H}$, τ_1, τ_2, τ_3, τ_4, γ

– **Estimate** the coefficients of the polynomial function f from $\mathbf{y}_\text{m}$ and $\mathbf{y}_\text{u}$ using the least-square method

REPEAT

1 - Estimate the Lipschitz constant L_{k+1} of $\mathbf{x} \mapsto \nabla_x H(\mathbf{x}, \mathbf{v^k})$ using the backtracking step size rule as in [6]

Update $\mathbf{x}$ using the analytical solution of [7]

$$\begin{aligned}\mathbf{x^{k+1}} &= \text{prox}^l_{L_{k+1}}\left(\mathbf{x^k} - \tfrac{1}{L_{k+1}}\nabla_x H(\mathbf{x^k}, \mathbf{v^k})\right)\\ &= \underset{\mathbf{x}}{\text{argmin}}\ \ \tfrac{1}{2}\|\mathbf{SHx} - \mathbf{y}_\text{m}\|^2 + \tau_1\|\nabla\mathbf{x}\|^2\\ &\quad + \tfrac{L_{k+1}}{2}\|\mathbf{x} - (\mathbf{x^k} - \tfrac{1}{L_{k+1}}\nabla_x H(\mathbf{x^k}, \mathbf{v^k}))\|^2\end{aligned}$$

2 - Set $d_k = 2\tau_4$ and update $\mathbf{v}$ using the gradient descent

$$\begin{aligned}\mathbf{v^{k+1}} &= \text{prox}^g_{d_k}\left(\mathbf{v^k} - \tfrac{1}{d_k}\nabla_v H(\mathbf{x^{k+1}}, \mathbf{v^k})\right)\\ &= \underset{\mathbf{v}}{\text{argmin}}\ \ \tau_2\textstyle\sum_i[\exp(y_{\text{u},i} - v_i) - \gamma(y_{\text{u},i} - v_i)]\\ &\quad + \tau_3\|\nabla\mathbf{v}\|^2 + \tfrac{d_k}{2}\|\mathbf{v} - (\mathbf{v^k} - \tfrac{1}{d_k}\nabla_v H(\mathbf{x^{k+1}}, \mathbf{v^k}))\|^2\end{aligned}$$

Until stopping criterion is satisfied

Output: Fused image $\mathbf{x}$

TABLE I: Contrast to noise ratios computed between two regions extracted from the beef steak and the PVA structure.

	MRI	US	Fused image
CNR	48.76 dB	20.64 dB	37.73 dB

TABLE II: Profiles' slope at the interfaces between different regions of interest in the MRI, US and fused images, corresponding to the vertical line in Fig. 1(b).

	MRI	US	Fused image
Interface 1 slope	$2.89e^{-2}$	$7.42e^{-2}$	$7.42e^{-2}$
Interface 2 slope	$-0.10e^{-2}$	$8.89e^{-2}$	$6.86e^{-2}$
Interface 3 slope	$3.57e^{-2}$	$5.47e^{-2}$	$6.61e^{-2}$
Interface 4 slope	$-1.35e^{-2}$	$-1.95e^{-2}$	$-2.05e^{-2}$

REFERENCES

[1] H. Roman, I. Chanavaz-Lacheray, M. Ballester, S. Bendifallah, S. Touleimat, J.-J. Tuech, M. Farella, and B. Merlot, "High postoperative fertility rate following surgical management of colorectal endometriosis," *Human Reproduction*, vol. 33, no. 9, pp. 1669–1676, 2018.

[2] D. Kundu and M. Z. Raqab, "Generalized rayleigh distribution: different methods of estimations," *Computational statistics & data analysis*, vol. 49, no. 1, pp. 187–200, 2005.

[3] T. Tuthill, R. Sperry, and K. Parker, "Deviations from Rayleigh statistics in ultrasonic speckle," *Ultrasonic imaging*, vol. 10, no. 2, pp. 81–89, 1988.

[4] A. Roche, X. Pennec, G. Malandain, and N. Ayache, "Rigid registration of 3D ultrasound with MR images: a new approach combining intensity and gradient information," *IEEE Trans. Med. Imaging*, vol. 20, no. 10, pp. 1038–1049, 2001.

[5] J. Bolte, S. Sabach, and M. Teboulle, "Proximal alternating linearized minimization or nonconvex and nonsmooth problems," *Mathematical Programming*, vol. 146, no. 1-2, pp. 459–494, 2014.

[6] A. Beck and M. Teboulle, "A fast iterative shrinkage-thresholding algorithm for linear inverse problems," *SIAM journal on imaging sciences*, vol. 2, no. 1, pp. 183–202, 2009.

[7] N. Zhao, Q. Wei, A. Basarab, N. Dobigeon, D. Kouamé, and J.-Y. Tourneret, "Fast single image super-resolution using a new analytical solution for l_2-l_2 problems," *IEEE Trans. Image Process.*, vol. 25, pp. 3683–3697, 2016.